TID-4500, UC-4
Chemistry

Lawrence Radiation Laboratory
UNIVERSITY OF CALIFORNIA
LIVERMORE

UCRL-50956

PRECIPITATION HARDENING OF Mo-1 at.% Hf BY INTERNAL NITRIDING

J. B. Mitchell
L. Himmel
J. S. Kane

Contents

PRECIPITATION HARDENING OF Mo-1 at.% Hf BY INTERNAL NITRIDING

Abstract

Precipitation hardening of 0.050-in.-thick sheets of a Mo-1 at.%Hf solid-solution alloy was accomplished by internal nitriding which produced a homogeneous dispersion of coherent plate-like HfN precipitates oriented on {001} planes of the molybdenum matrix. The high-temperature tensile strength of this alloy is substantially superior to that of TZM and TZC.

During internal nitriding, growth of the HfN particles occurs at the advancing nitriding front by Ostwald ripening which produces an increase in average particle size with increasing depth below the external surface. The high nitrogen activity in the alloy behind the nitriding front effectively inhibits dissociation and growth of the precipitates. The plate-like HfN particles grow in diameter in a coherent manner. Thickening of the particles occurs by the nucleation and growth of coherent ledges on the planar surfaces. This thickening process produces an increase in the coherency strain which is relaxed by the formation of intrinsic dislocation loops within the particles by the coalescence of vacancies. The large HfN particles developed by this growth mechanism retain substantial coherency strain. A severe particle-coarsening mechanism is operative at high temperatures in regions of the nitrided alloy containing a high density of small fully coherent precipitates. The coarsening occurs by the migration of grain boundaries which sweep up the small fully coherent precipitates, the components of which then feed large semicoherent particles growing behind the boundary.

Introduction

It is well known that certain oxides, carbides and nitrides of the group IV elements have superior thermochemical stability, and these have been used as dispersions in the development of precipitation-hardened bcc refractory alloys for service at temperatures above the useful range of superalloys. Two notable examples of commercial, high-strength, precipitation-hardened molybdenum-base alloys utilizing titanium and zirconium carbide dispersions, together with thermal-mechanical processing for their strength, are TZM and TZC.

Several years ago, Mukherjee and Martin[1] established that dilute solid tions of Ti and Zr in Mo could be selectively internally-nitrided to produce a

dispersion of nitride particles that significantly enhanced the strength of Mo.

More recently, Ryan and Martin[2] investigated precipitation-hardening of Mo with carbides and nitrides of Ti, Zr and Hf by quench-aging. They reported that whereas homogeneous precipitation of all these phases occurred by formation of coherent plate-like particles on habit planes of the Mo matrix, the compounds of Ti and Zr tended more generally to precipitate heterogeneously on lattice defects, while the Hf compounds exhibited a finer, more homogeneous precipitation and produced a greater increase in hardness. These results suggest that precipitation-hardening of the Mo-Hf system by internal nitriding might be an attractive method of developing high-temperature properties superior to those currently available in commercial Mo-base alloys. The study reported here was begun to investigate the structures and mechanical properties produced in a Mo-1 at.% Hf alloy by internal nitriding.

Experimental Procedure

The Mo-Hf alloy was vacuum-arc-cast, hot-extruded, and rolled at about 1300°C to a final thickness of 0.055 in. This material was supplied in two different work-hardened conditions. Sheet A received a final rolling reduction corresponding to 55% hot-cold work. Sheet B was given a 70% reduction in the final rolling. Both sheets were stress-relieved for 1 hr in vacuum at 1230°C. The TZM and TZC were supplied as 0.060-in.-thick sheets stress-relieved 1 hr in vacuum at 1100°C. These materials were of standard composition and received standard (optimum) thermomechanical processing. Tensile specimens with 1-in.-gauge sections were machined from the sheet stock, ground and lapped to a thickness of 0.050 in. and diamond-polished. To prevent excessive recrystallization during nitriding, the Mo-Hf specimens were given an additional 2 hr recovery anneal in vacuum ($< 10^{-7}$ Torr) at 1325°C. The tensile specimens were then nitrided to completion under 1 atm N_2 for 290 hr at 1260°C, 186 hr at 1310°C and 72 hr at 1410°C, the required times having been established during preliminary studies of the diffusion-controlled nitriding kinetics. Several small coupons of the alloys were nitrided with the tensile specimens. These were used for microhardness measurements and metallographic and electron microscopy examinations. Thin foils for transmission microscopy were spark-machined from various depths in the specimen cross section and electropolished in a solution of 60 vol% methyl alcohol, 36 vol% butyl-cellosolve and 6 vol% perchloric acid using the window technique. Tensile tests were carried out on all specimens from 1100° to 1500°C in vacuum ($< 5 \times 10^{-6}$ Torr) at a strain rate of 0.01 in./min.

Discussion of Internal Nitriding Characteristics

The internal nitriding process is analogous to internal oxidation,[3] and proceeds by the diffusion-controlled advance of a nitriding front which remains essentially parallel to the external surface. At the advancing nitriding front, the inward diffusion of nitrogen and the outward diffusion of the alloyed Hf continuously provide concentrations in excess of those corresponding to the solubility product of HfN in the Mo matrix. A repeated nucleation and some accompanying growth of HfN particles results. The successful application of internal nitriding requires that the solute metal nitride form from solid solution at a nitrogen activity well below that at which nitrides of the base metal form. In addition, the nitrogen must have a rapid rate of transport in the base metal matrix, and greatly exceed that of the solute element. These two conditions are well satisfied in the Mo-Hf alloy. The diffusivity of nitrogen in Mo is approximately three orders of magnitude greater than that of Hf, and HfN is very stable whereas Mo_2N is unstable at the temperatures and nitrogen pressures selected for internal nitriding. The depth of the nitriding front, ξ, is a parabolic function of time given by

$$\xi = 2\gamma(D_N t)^{1/2} \qquad (1)$$

where γ is a constant and D_N is the diffusivity of nitrogen in Mo. The rate of advance of the nitriding front is given by

$$\frac{d\xi}{dt} = \gamma\left(\frac{D_N}{t}\right)^{1/2} \qquad (2)$$

and thus decreases with time or depth and increases with increasing temperature. The above equations were verified by experimental measurements of the nitriding rate at several temperatures as part of a more detailed study of the kinetics of internal nitriding of the Mo-Hf system, to be reported at a later date. Figure 1 shows the cross section of a Mo-1 at.% Hf specimen that was partially internally nitrided at 1360°C under 1 atm N_2 pressure for 4 hr. The nitriding front has advanced approximately 0.006 in. below the external surface during the anneal. The microhardness profile shows a substantial hardening of the alloy by the HfN precipitates behind the nitriding front which decreases with increasing depth. At the nitriding front, the hardness falls abruptly to that for the solid-solution alloy.

OBSERVATION OF MICROSTRUCTURE

A representative example of the microstructure and microhardness profile over the cross section of the Mo-1 at.% Hf alloy internally nitrided to completion is shown in Fig. 2 for a 0.050-in.-thick specimen of sheet A nitrided at 1360°C. Also shown in this figure are the microhardness profiles of specimens of sheet A nitrided at 1260°, 1310° and 1410°C. The HfN precipitate distribution is uniformly homogeneous over the entire cross section; however, the particle size, grain structure and microhardness show a significant variation with depth below the surface. Maximum hardness is observed

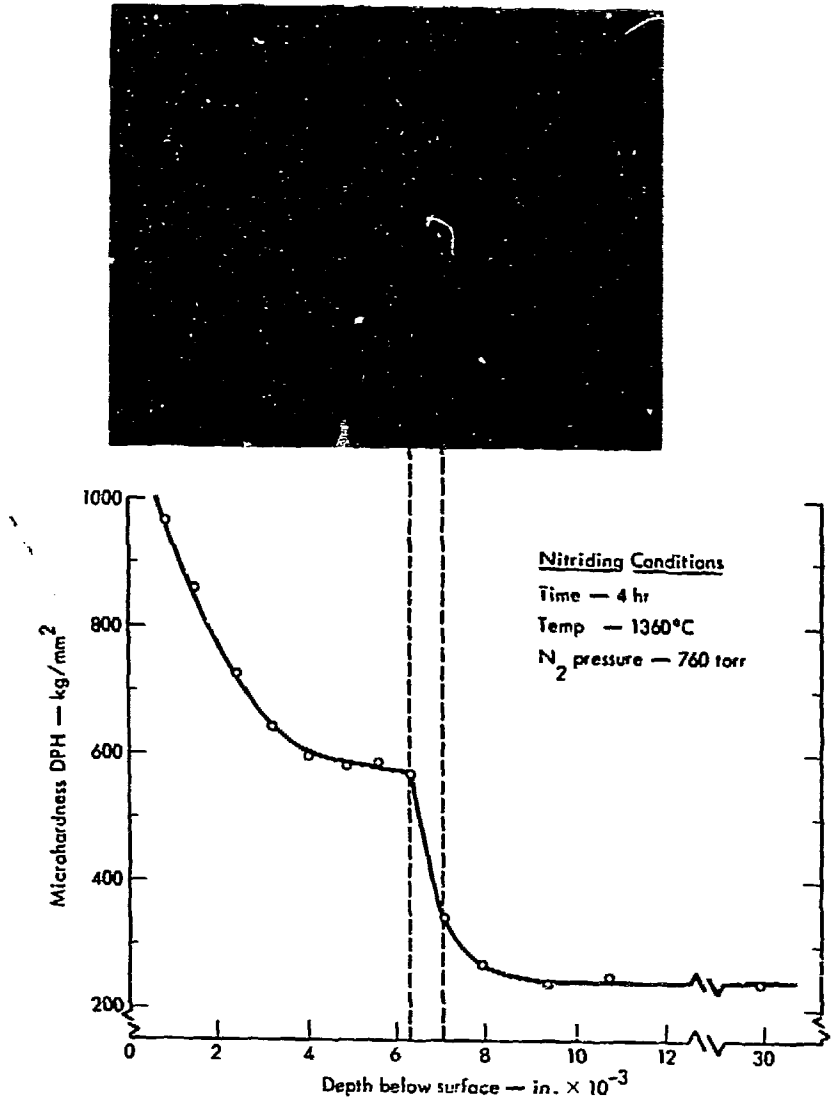

Fig. 1. Cross section of Mo-1 at.% Hf alloy, partially internally nitrided at 1360°C, showing nitriding front and microhardness profile.

approximately 0.003 in. below the surface, corresponding to a structure of work-hardened elongated grains containing very small HfN precipitates (not resolved in Fig. 2). With increasing depth the hardness decreases, the HfN particle size

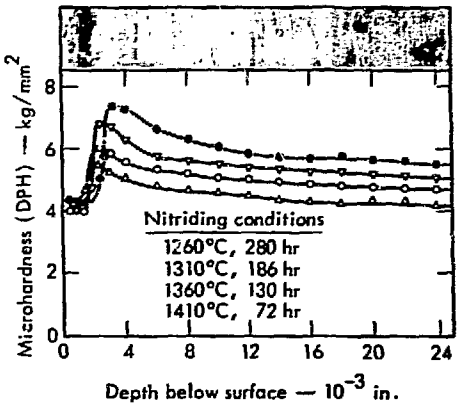

Fig. 2. Cross-section microstructure and microhardness profiles of fully nitrided Mo-1 at.% Hf alloy.

increases, and the grain structure exhibits an increasing degree of recovery of work-hardening. Finally, a region of relatively low hardness and a coarse dispersion of very large HfN particles in small pseudo-equiaxed grains extends from the surface to a depth of approximately 0.003 in. Figures 3 through 8 show the cross-section microstructures near the surface and at the center of the specimens from sheets A and B nitrided at 1260°, 1310° and 1410°C. These photographs reveal the variation in microstructure to be qualitatively the same as that described in Fig. 2. Comparison of the structures of specimens from the same sheet nitrided at the three temperatures shows that the lower nitriding temperatures generally produce smaller precipitates, less recovery of the work-hardened structure, and a deeper subsurface region of coarse precipitates. The variations in structure with nitriding temperature are reflected in the microhardness profiles in Fig. 2 where it can

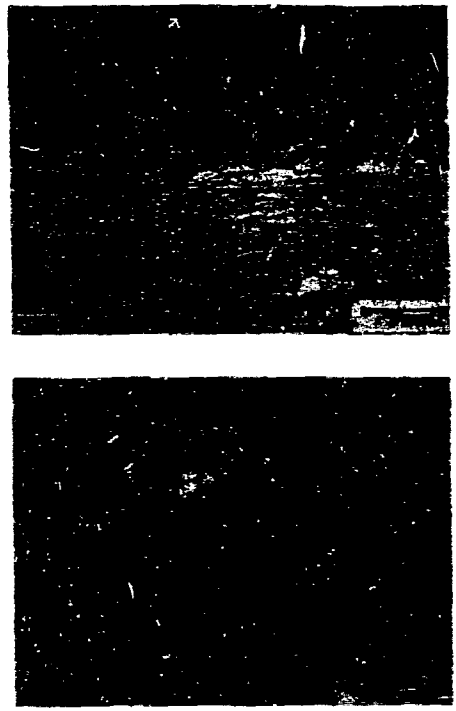

Fig. 3. Cross-section microstructures near the surface and at the center of specimen of sheet A internally nitrided at 1260°C.

be seen that the lower nitriding temperatures produce a higher average hardness and a deeper subsurface zone of lower hardness. Comparison of the microstructures of specimens of sheets A and B nitrided at the same temperature reveals the particle size distribution to be essentially identical, but a significantly greater degree of recovery of work-hardening has occurred in specimens of sheet B.

Figures 9 and 10 are transmission electron micrographs of the internal

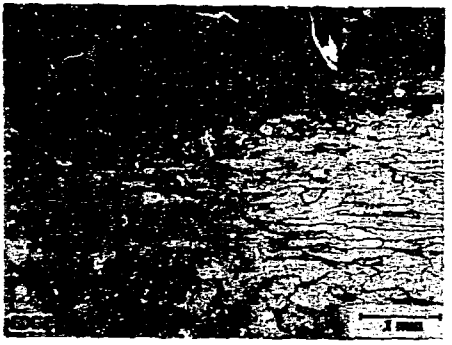

Fig. 4. Cross-section microstructures near the surface and at the center of specimen of sheet B internally nitrided at 1260°C.

Fig. 5. Cross-section microstructures near the surface and at the center of specimen of sheet A internally nitrided at 1310°C.

structure approximately 0.005 in. below the surface of a specimen of sheet A nitrided at 1310°C. These micrographs show matrix strain and displacement fringe contrast arising from peripheral coherency at small plate-like HfN precipitates. The platelets are less than 20 Å thick and from 100 to 500 Å in diameter. The selected area diffraction pattern in Fig. 9 exhibits streaking in the ⟨100⟩ directions of the Mo matrix, characteristic of thin plate-like particles oriented on {001} planes of the Mo matrix as shown schematically in Fig. 11a. The matrix strain contrast near the precipitates using the ⟨200⟩ matrix reflections in dark field indicates a positive peripheral lattice misfit (dark contrast on the side of positive g vector) where the Mo lattice is compressed normal to the plane of the platelets, as illustrated in Fig. 11b. This peripheral coherency strain undoubtedly makes a major contribution to the high hardness observed at this depth in the specimen cross section. An additional contribution to the hardness at this depth is also expected from the work-hardened structure developed during rolling of the

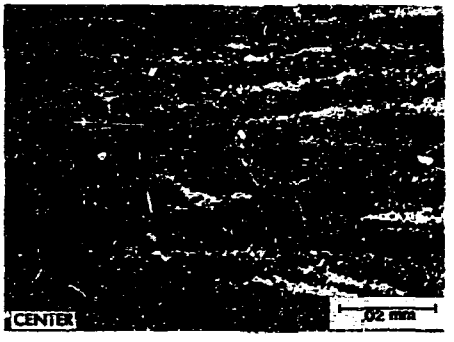

Fig. 6. Cross-section microstructures near the surface and at the center of specimen of sheet B internally nitrided at 1310°C.

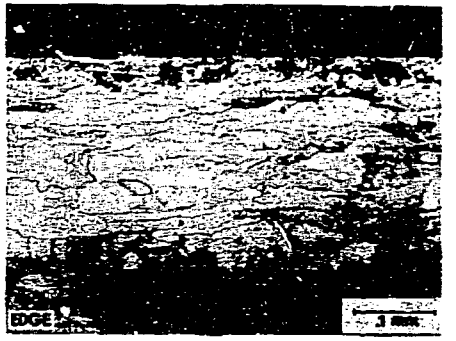

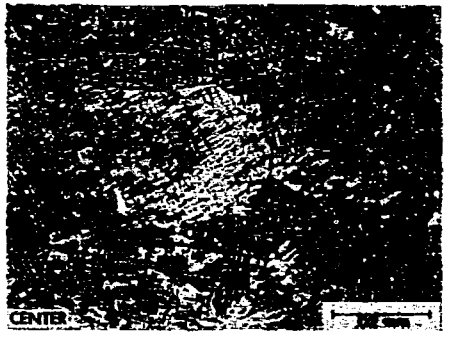

Fig. 7. Cross-section microstructures near the surface and at the center of specimen of sheet A internally nitrided at 1410°C.

sheet stock. Figure 12 shows the retained substructure which consists of polygonized subgrains approximately 1 μ in diameter. The subgrain boundaries contain a high density of precipitates, and are bounded by narrow denuded zones. Comparison of this substructure with that of the as-received, solid-solution alloy shown in Fig. 13 reveals that only a modest amount of recovery has occurred at this depth in the cross section during the nitriding anneal. The HfN precipitates formed in the subbcundaries early enough in the anneal to lock in (stabilize) the substructure before extensive recovery occurred. These small precipitates, having formed early in the nitriding anneal, were subjected to a temperature of 1310°C for approximately 170 hr without exhibiting significant coarsening or loss of coherency. Thus the high nitrogen activity in the alloy behind the nitriding front effectively inhibits dissociation and growth of the precipitates by Ostwald ripening. Consequently, the precipitates grow only at the advancing nitriding front, and their

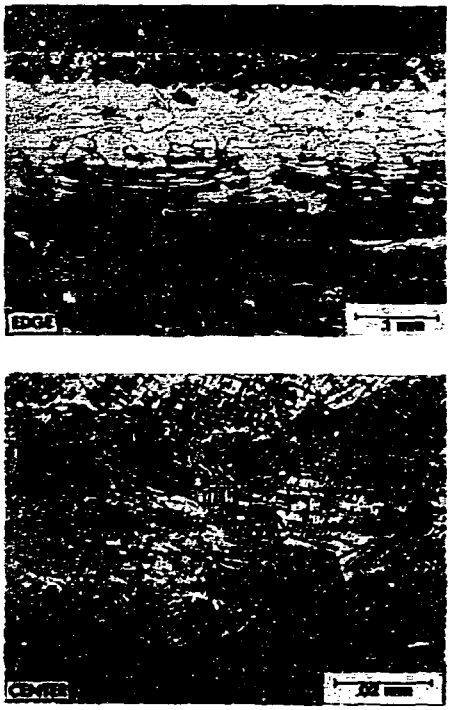

Fig. 8. Cross-section microstructures near the surface and at the center of specimen of sheet B internally nitrided at 1410°C.

Fig. 9. Transmission micrograph showing matrix strain contrast near coherent HfN precipitates at a depth of 0.005 in. after nitriding at 1310°C.

size at a given depth in the cross section is determined by the time available for growth during passage of the front.

The increase in particle size with increasing depth is a direct consequence of the decrease in the rate of advance of the nitriding front with increasing depth.

Transmission micrographs of the precipitates at depths of 0.015 and 0.025 in. below the surface after nitriding at 1310°C are shown in Figs. 14 through 16. The particles generally exhibit a wide variation in size. The larger particles are circular platelets approximately 20 to 60 Å thick and several thousand angstroms in diameter. Their rectangular appearance in Figs. 14 and 15 is caused by their intersection with the top and bottom (111) surfaces of the Mo foil. These large precipitates show strong displacement fringe contrast in Figs. 14 and 15 and compressive matrix strain contrast in Fig. 16, indicating that they still retain substantial peripheral coherency with the Mo matrix. Only two of the three particle orientations in Figs. 14 and 15 show displacement fringe contrast. The particles in the third orientation on (010) matrix planes produce a [010] peripheral displacement vector, R_n,

Fig. 10. Transmission micrograph showing displacement fringe contrast on HfN precipitates at a depth of 0.005 in. after nitriding at 1310°C.

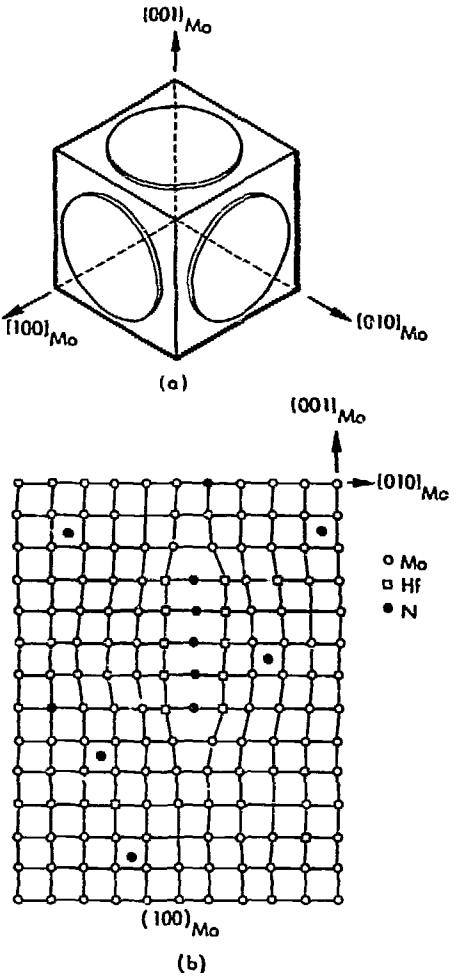

Fig. 11. Schematic illustration of morphology of coherent HfN precipitates.

which is normal to the operating $[10\bar{1}]$ matrix, g, reflection. Therefore, $g \cdot R_n = 0$, and these particles are consequently out of contrast. Selected area diffraction patterns in regions containing these larger particles exhibited weak secondary spots which as shown in the dark field micrographs in Fig. 17 were produced by diffraction from the HfN particles. Analysis of these secondary spot patterns, together with dark field experiments, revealed the crystallographic precipitate-matrix orientation relationship illustrated in Fig. 18. This orientation relationship agrees with that determined by Ryan and Martin[2] from moiré pattern analysis. It is evident from Fig. 18 that the lattice mismatch for a fully coherent precipitate platelet results in a large positive misfit normal to the plane of the plate and a small positive misfit in the plane.

Fig. 12. Transmission micrograph of dislocation cell structure at a depth of 0.005 in. after nitriding at 1310°C.

Fig. 13. Transmission micrograph of substructure in as-received Mo-1 at.% Hf solid solution alloy.

Figures 14 and 15 reveal that the displacement fringe contrast changes abruptly across dislocation loops that appear to grow in the plane of the particles. Within some of the loops at A, the intensity of the displacement fringes increases while within other loops at B, the fringes are very weak and in some cases totally absent. The change in displacement fringe intensity within these loops indicates that the magnitude of the peripheral coherency strain is changed by the growth of the loops. Thus the nucleation and growth of these loops appear to play an important role in the growth and degree of coherency of the HfN particles.

The transmission micrographs in Figs. 19 through 25 show the precipitate morphology near the nitriding front in a specimen that was partially nitrided to a depth of approximately 0.020 in. at 1310°C. Figure 19 shows a region containing particles approximately 600 Å in diameter which contain a small loop. The contrast near the loop is somewhat complicated by the displacement fringes and a light circular fringe adjacent to the darker loop image. The light circular fringe is similar to those observed on coherent precipitates in Ni-Cr-Ti-Al alloys[4] and probably results from interface

Fig. 14. Transmission micrograph of HfN particles at a depth of 0.015 in. after nitriding at 1310°C.

Fig. 15. Transmission micrograph of HfN particles at a depth of 0.025 in. after nitriding at 1310°C.

contrast caused by curvature of the precipitate-matrix interface near the loop. Several of the particles at P in Fig. 19 have grown to approximately 5000 Å in diameter, and the loop has grown in the plane of the particles. Another area showing the particle in the more advanced stage of growth is shown in Fig. 20 where it can be seen that the intensity of the displacement fringes is generally stronger within the loop. The increase in fringe intensity indicates that the compressive peripheral coherency displacement normal to the plane of the precipitate is increased by growth of the loop. Thus, these loops appear to be extrinsic in nature. Figure 21 shows the precipitates as viewed along the [001] matrix direction. The particles lying in the plane of the photograph can be seen to contain one or more loops. Both the precipitate and the loop images display a line of no contrast normal to the operating [020] g vector, characteristic of intrinsic or extrinsic edge dislocation loops with Burger's vector normal to the plane of the loop.

The loops in Figs. 19 and 20 appear to be coherent ledges that nucleate and grow on the surface of the particles and constitute the mechanism of thickening, as illustrated in Fig. 22. The growth of these extrinsic coherent ledges causes the compressive peripheral coherency

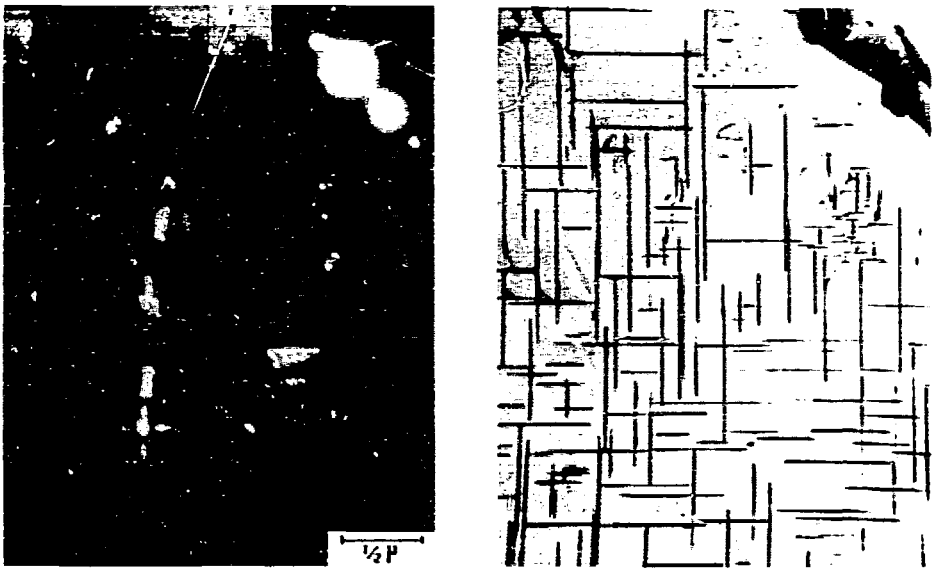

Fig. 16. Bright and dark field transmission micrographs showing precipitate and matrix stream contrast at a depth of 0.025 in. after nitriding at 1310°C.

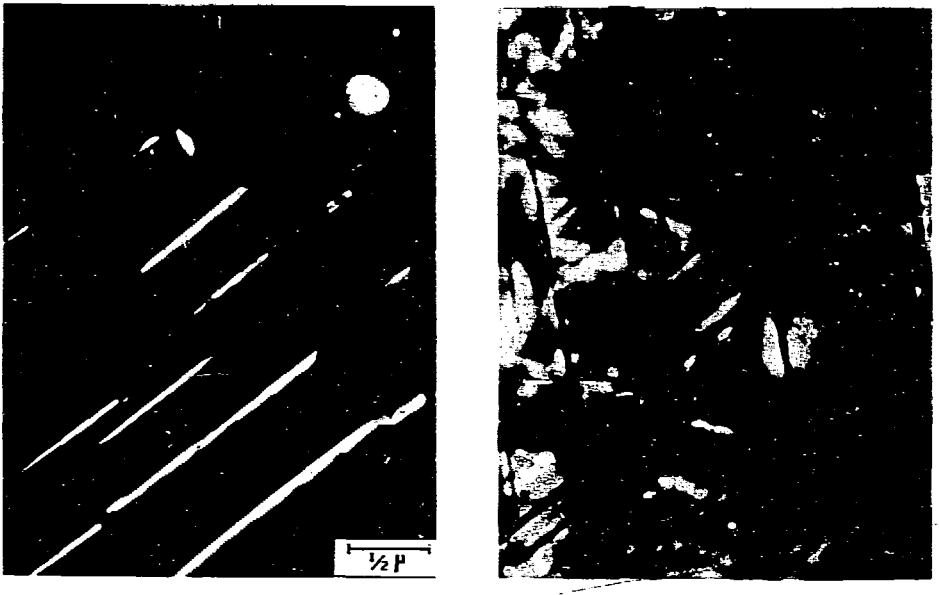

Fig. 17. Bright and dark field transmission micrographs illustrating diffraction by HfN precipitates at a depth of 0.025 in. after nitriding at 1310°C.

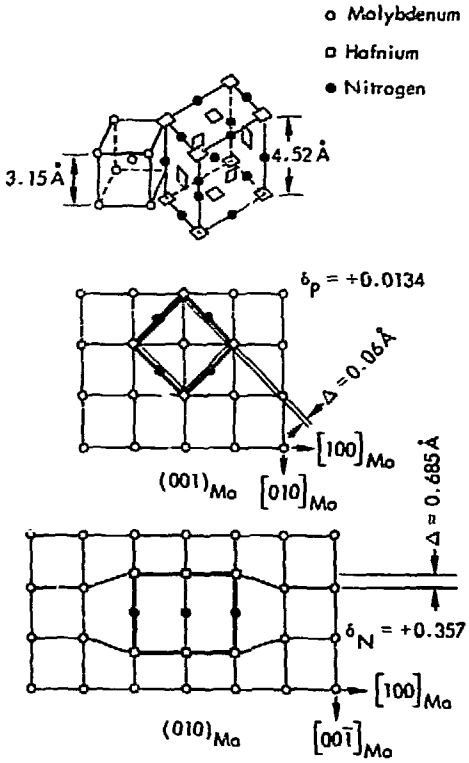

Fig. 18. Schematic illustration of crystallographic precipitate-matrix orientation relationship.

Fig. 19. Transmission micrograph showing loops on HfN precipitates near the nitriding front at a depth of 0.020 in. after nitriding at 1310°C.

strain in the matrix to increase, producing an increase in displacement fringe intensity. The ledge illustrated in Fig. 22 has a height of one HfN unit cell and the magnitude of the associated normal displacement vector is 1.37 Å. The magnitude of the displacement vector of the loops in Figs. 19 and 20 is not known. These loops appear to be the first to form on the particles. They never grow completely to the periphery of the particles and were seen as the outermost loop on all the large particles observed in this study. As shown at B in Figs. 19 and 23, several of the precipitates at this stage of growth contain a second loop which has formed inside the first loop. Within this second loop the displacement fringes are extremely weak or totally absent. The disappearance of the displacement fringes within the second loop suggests that $g \cdot R_n$ is an integer. Thus the development of the second extrinsic ledge may have produced a peripheral coherency displacement equal to the ⟨001⟩ Burger's vector in the Mo matrix.

Another explanation for the contrast is that the second loop is an intrinsic dislocation loop formed within the HfN particles by the coalescence of vacancies, as

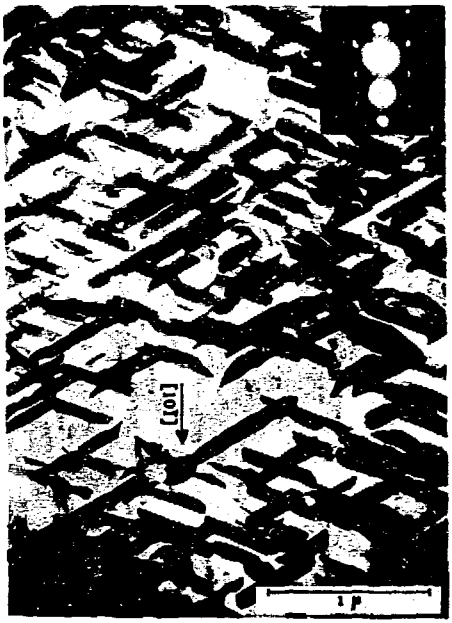

Fig. 20. Transmission micrograph of larger particles containing a single loop at a depth of 0.020 in.

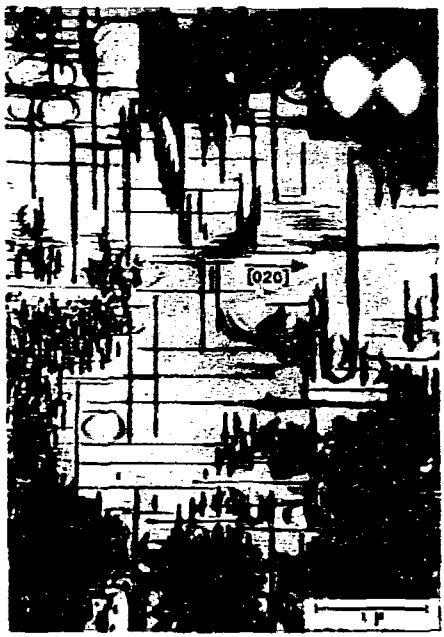

Fig. 21. Transmission micrograph showing precipitate and loop contrast in [001] orientation at a depth of 0.020 in.

illustrated in Fig. 24. As shown in the figure, growth of this loop relaxes the peripheral coherency strain so that within the loop the peripheral displacement R_n is small and the displacement fringe intensity is weak. Precipitates containing the second loop viewed along the ⟨001⟩ matrix direction are shown in Fig. 25. The irregular edge of a precipitate lying in the plane of the photograph can be seen at P, the extrinsic ledge loop at A, and the second loop at B. The edge view of these particles at J shows matrix strain contrast only near the ends of the particles, as would be expected to result from the growth of the intrinsic loop in Fig. 24.

Thus both the displacement fringe and matrix strain contrast are consistent with an intrinsic second loop. Assuming that the peripheral lattice mismatch is compensated entirely by the compressive strain in the Mo matrix and that the matrix strain is completely relaxed within the intrinsic loop, the thickness of the HfN precipitate, Δt, can be estimated from the relation

$$\Delta t \left(\frac{a_2 - a_1}{a_2} \right) - a_2 \approx 0 \qquad (3)$$

where a_1 and a_2 are the ⟨001⟩ unit cell dimensions of Mo and HfN respectively.

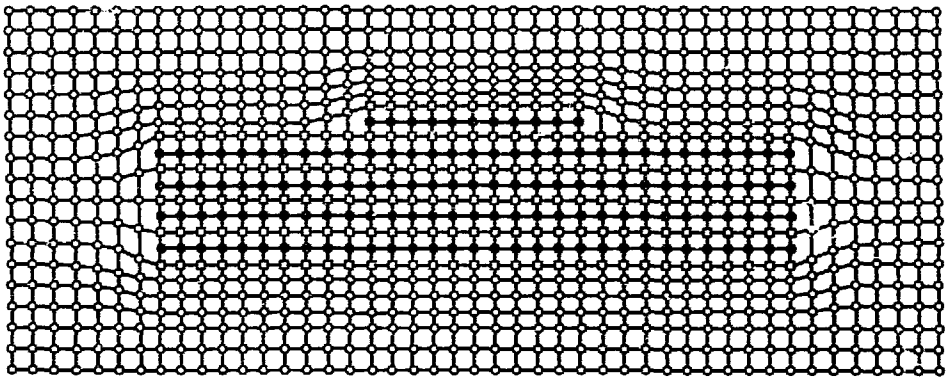

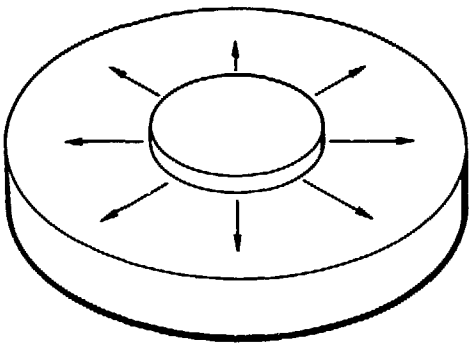

Fig. 22. Schematic illustration of particle thickening by the growth of a coherent ledge.

Using the values of a_1 and a_2 in Fig. 18 gives $\Delta t \approx 15$ Å or three to four unit cells thick, which is in agreement with the 20 Å thickness estimated from the transmission micrographs.

A more advanced stage of particle growth is shown in Fig. 26 where it can be seen that several more loops at C, D and E have formed concentrically within the first two loops. The consecutive growth of these new loops has restored the displacement fringes which were removed by the growth of the intrinsic loop B. Within these loops the growth of another loop at F has removed the fringes. Loop F is then followed by loop G which

Fig. 23. Transmission micrograph of precipitates containing two loops in [111] orientation at a depth of 0.020 in.

again restores the displacement fringe contrast.

The growth sequence of three fringe-restoring loops between two fringe-removing loops was observed on all of the large precipitates, and on occasion a sequence of four fringe-restoring loops between two fringe-removing loops was observed. The fringe-restoring loops C, D and E appear to be coherent ledges similar to loop A. The consecutive nucleation and growth of these ledges within the intrinsic loop B thickens the precipitate and increases the periphery coherency strain in the matrix which increases the displacement fringe intensity. Further thickening of the particle requires that this peripheral coherency strain be relaxed, which occurs by the nucleation and growth of another intrinsic loop F. The thickening sequence of three extrinsic ledges followed by an intrinsic

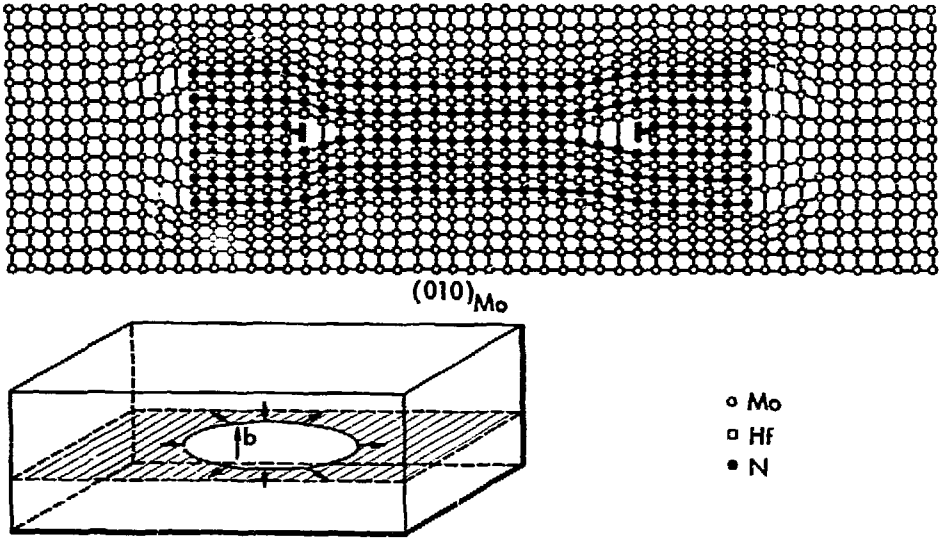

Fig. 24. Schematic illustration of relaxation of pheripheral coherency strain by the growth of an intrinsic dislocation loop.

Fig. 25. Transmission micrograph of HfN precipitates containing two loops in [001] orientation at a depth of 0.020 in.

Fig. 26. Transmission micrograph showing loop growth sequences on large HfN particles at a depth of 0.025 in. after nitriding at 1310°C.

loop then starts over again, as shown on the large particle at R in Fig. 16, where the loop growth sequence is repeated several times. The formation of three to four extrinsic ledges between two intrinsic loops indicates that the particle ledges are one HfN unit cell high. An increase of three to four HfN unit cells in particle thickness produces a peripheral coherency lattice displacement of from 4.11 to 5.48 Å, which on the average is approximately the displacement relaxation produced by an intrinsic loop with a Burger's vector of 4.57 Å.

These observations indicate that the HfN precipitates grow in the Mo matrix in a manner such that the precipitate-matrix interface is always fully coherent, as illustrated in Fig. 27. The figure shows the particles on edge at several stages of growth. Initially, the HfN particles probably develop at the nitride front by Hf-N clustering in the molybdenum matrix similar to that observed for Zr-N in niobium.[5] Small coherent HfN platelets 1 to 2 unit cells thick grow homogeneously from these clusters on {001} planes of the matrix. When they reach a size of approximately 15 to 20 Å thick and 200 to 300 Å in diameter, further thickening occurs by the nucleation and growth of a coherent ledge on the surface of the particle which appears as a dislocation loop. The ledge grows in diameter along with the coherent diametral growth

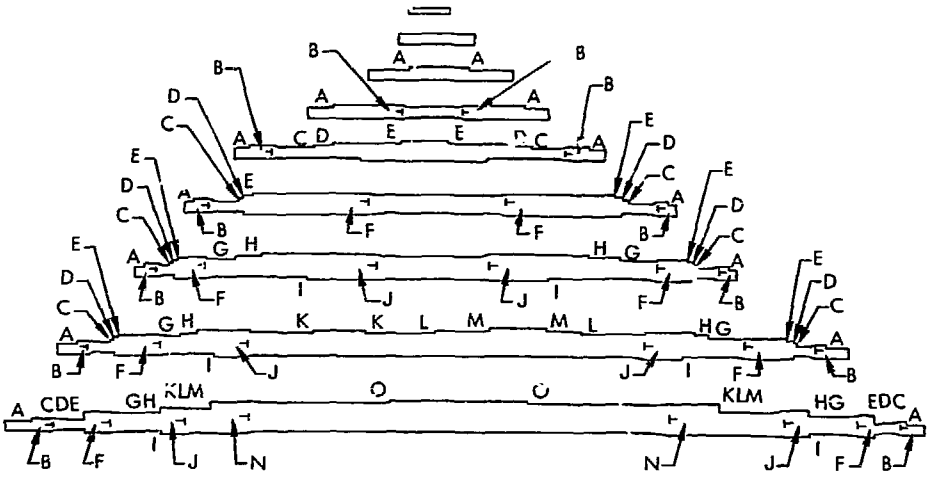

Fig. 27. Schematic illustration of thickening and coherency loss mechanisms during growth of HfN particles.

of the particle to 4000 to 5000 Å. At this stage, a second intrinsic loop forms within the particle that relaxes the peripheral coherency strain. With continued diametral growth of the particle, thickening occurs by the repeated sequence of concentric growth of three to four extrinsic ledge loops and an intrinsic loop. The large particles developed by this growth process retain a significant amount of peripheral coherency strain. When the particles get very large, the ledges nucleate at more than one place on the particle surface and the loop geometry becomes very complex as at S in Figs. 15 and 26. Near the outer edge of these large particles the ledges appear to coalesce into steps, as shown at T in Fig. 28.

As previously described, growth of the HfN particles during internal nitriding occurs almost exclusively at the nitriding front. The decrease in rate of advance

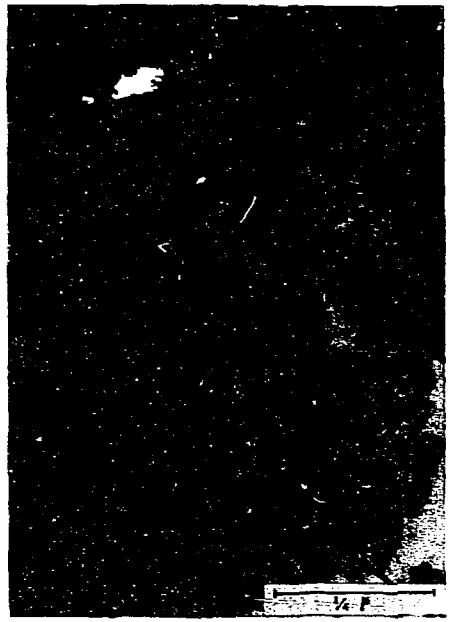

Fig. 28. Transmission micrograph of steps on large HfN particles at a depth of 0.025 in. after nitriding at 1310°C.

of the front with increasing depth below the external surface allows the particles at greater depths more time to grow to a larger size. The nature and distribution of the precipitates shown in the electron-micrographs indicates that the principal mechanism of growth is Ostwald ripening where some particles grow at the expense of others which dissolve into the matrix. Figure 19 shows an area near the nitriding front at a depth of approximately 0.020 in. containing small precipitates of uniform size and distribution. Several larger particles have preferentially grown at P around which are denuded regions, suggesting that some of the neighboring smaller particles dissolved during their growth. Figure 21 shows another area near that of Fig. 19 where the general distribution of the precipitates is characteristic of that expected during Ostwald ripening. Further evidence of particle dissolution can be seen at L in Figs. 14 and 15 where some particles apparently in the final stages of dissolution have fragmented into many small loops. It is evident that the dissociation and dissolution of the HfN particles can occur only at the nitriding front where the activity of nitrogen and hafnium in the matrix has been decreased by the precipitation. Once the nitriding front has passed a given depth in the specimen, the precipitate size and distribution at that depth are effectively frozen in by the increased nitrogen activity behind the front. Consequently, the particle growth by Ostwald ripening occurs almost simultaneously with the precipitation at the nitriding front. The precipitate distributions shown at increasing depths in Figs. 14 and 15 are essentially those of more advanced stages of Ostwald ripening.

Fig. 29. Transmission micrograph of subsurface particle coarsening.

Figure 29 shows the particle coarsening that occurs to a depth of from 0.002 to 0.003 in. below the surface of the fully nitrided specimens. The mechanism responsible for this coarsening is shown in Fig. 30. Some time after the passage of the nitriding front, grain boundaries such as the one at M in Fig. 30 migrate across the grains, sweeping up or absorbing the small HfN precipitates, the components of which then feed large particles growing behind the boundary. The large particles formed by this process exhibit many edge dislocation loops (see Fig. 31a) and a second dislocation network on the planar surface (see Fig. 31b) indicating that they

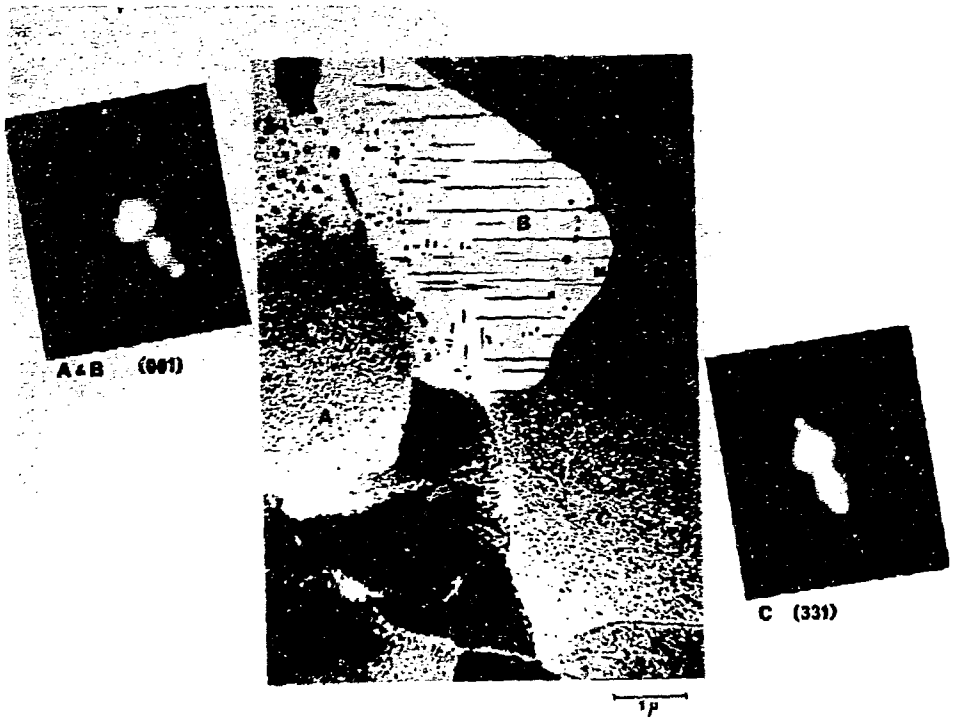

Fig. 30. Transmission micrograph illustrating mechanism of subsurface particle coarsening.

have only a small degree of coherency. The driving force of this process is the reduction in coherency strain energy associated with the small, fully coherent precipitates. This coarsening process occurs to an equal extent in specimens that have been fully recrystallized prior to nitriding (see Fig 32a) and is operative only in regions where small, fully coherent HfN particles are present, such as adjacent to open cracks penetrating into the center of the specimen, as shown in Fig. 32b. Since smaller precipitates are formed to a greater depth at lower nitriding temperatures, the coarsening occurs to a greater depth as the nitriding temperature is lowered.

TENSILE PROPERTIES

Tensile stress-strain curves at 1100°C for the Mo-1 at.% Hf alloy in the recovered solid-solution condition and after internal nitriding at 1260°C are shown along with that for TZM in Fig. 33. It is evident in this figure that the HfN precipitation produces a marked increase in tensile strength.

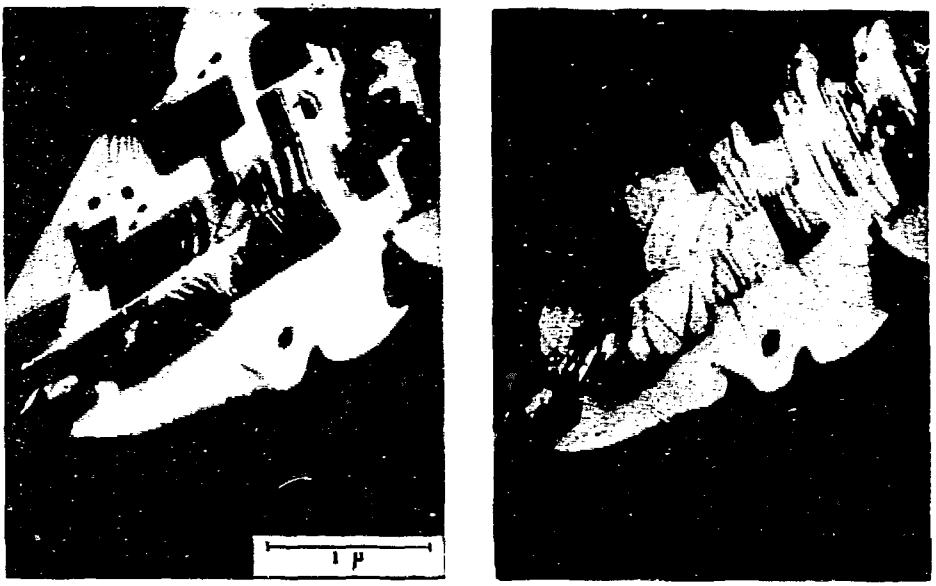

Fig. 31. Transmission micrograph of large HfN particles produced by coarsening mechanism showing dislocation networks.

Figures 34 and 35 show the 0.2% offset yield strength and ultimate tensile strength at elevated temperatures for the Mo-1 at.% Hf alloys TZM and TZC. The high-temperature tensile strengths of the nitrided Mo-Hf alloy are in general substantially superior to those of TZM and TZC. At 1100°C the highest strength nitrided alloy is approximately twice that of TZM and TZC, and six times stronger at 1500°C.

The internally-nitrided Mo-Hf alloy also exhibits superior strength stability at high temperatures. When TZM was subjected to a temperature of 1300°C for 2 hr in vacuum, its yield strength at 1100°C decreased from 58 ksi to 42 ksi due to recovery of the work-hardened structure developed during the thermo-mechanical processing. In contrast, the nitrided alloys exhibited only a very modest loss of strength when annealed in vacuum at higher temperatures for longer times. The observed high thermochemical stability of the small HfN precipitates behind the nitriding front where the nitrogen activity in the matrix is high indicates that the high-temperature strength of the nitrided alloy should be exceptionally stable relative to coarsening of the precipitates when used in a nitrogen environment.

As shown in Figs. 34 and 35, lower nitriding temperatures produce higher tensile strength. This behavior is in accord with the increase in hardness with decreasing nitriding temperatures, shown in Fig. 2. The principal factor responsible for this behavior is probably the

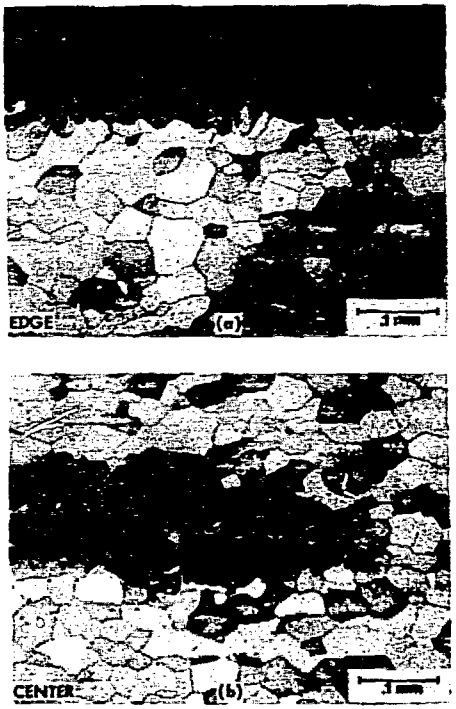

Fig. 32. Subsurface particle coarsening in a specimen that was fully recrystallized prior to nitriding.

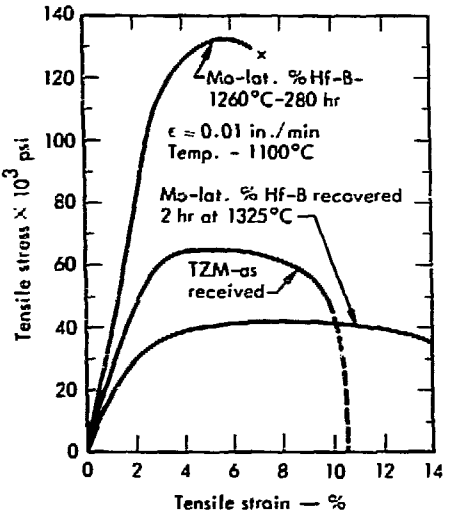

Fig. 33. Tensile stress-strain curves for Mo-1 at.% Hf and TZM at 1100°C.

finer particle dispersions observed in specimens nitrided at the lower temperature. Part of the increase in strength is due to less recovery of the work-hardened substructure at the lower nitriding temperatures.

Comparison of the tensile data for specimens from sheets A and B at the same nitriding temperature shows that an additional improvement in strength is obtained from retained work-hardening. The as-received Mo-Hf alloy of sheet B which contained 70% hot-cold work exhibited substantial recovery when annealed for 2 hr in vacuum at 1325°C, as shown in the tensile data at 1100°C. Specimens of sheet A which contained 55% hot-cold work exhibited only a minor decrease in strength after 8 hr at 1325°C. Thus, the higher strength of specimens of sheet A is attributable to retained work-hardening. This conclusion is supported by the metallographic observations in Figs. 3 through 8 that less recovery of the work-hardened structure occurred in specimens of sheet A during internal nitriding.

The observed variation in precipitate size and microhardness over the cross section of the internally nitrided Mo-Hf specimens indicates that the tensile properties are not the optimum obtainable. A significant improvement in the strength of this alloy might be made by controlling the rate of advance of the nitriding front by varying the temperature or nitrogen pressure during nitriding so as to develop

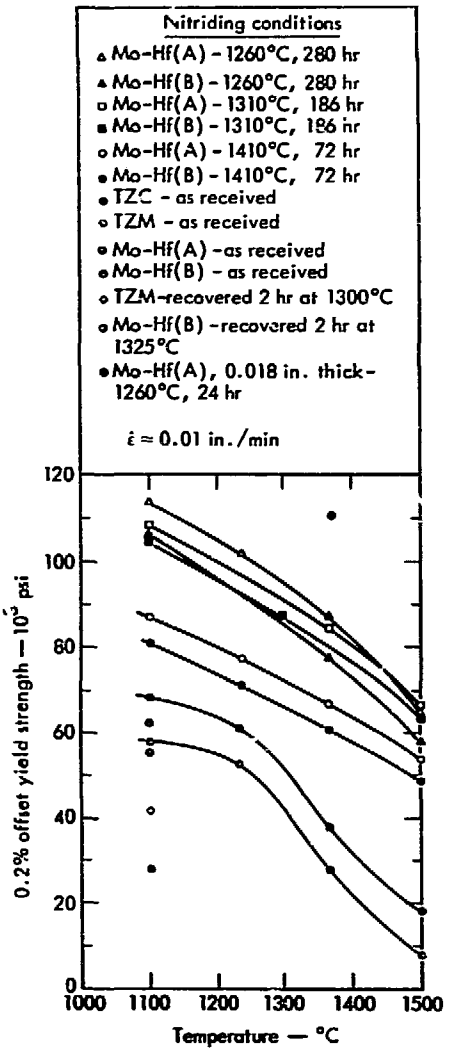

Fig. 34. 0.2% offset yield strength versus temperature for internally nitrided Mo-1 at.% Hf TZM and TZC.

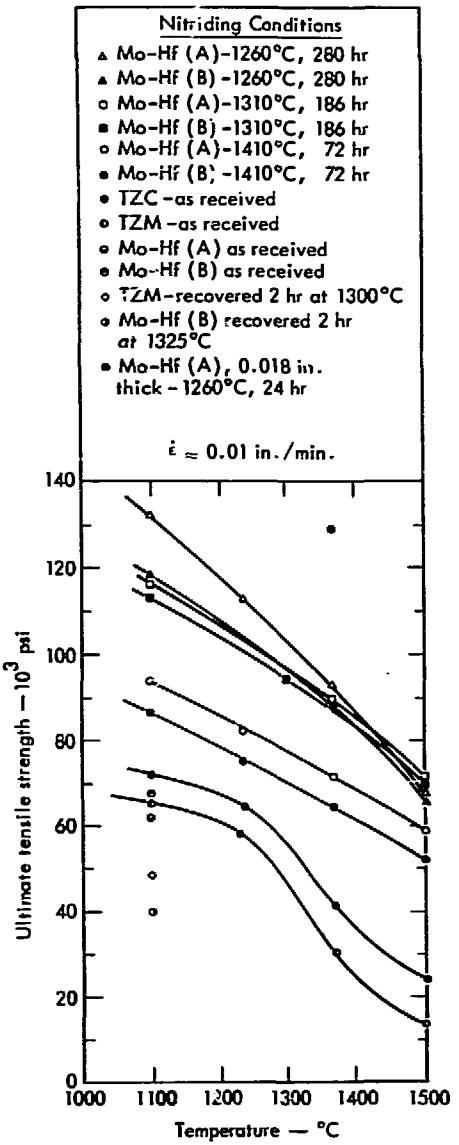

Fig. 35. Ultimate tensile strength versus temperature for internally nitrided Mo-1 at.% Hf TZM and TZC.

a uniform optimum particle size over the cross section. In addition, some improvement in mechanical properties might be achieved by varying the Hf solute concentration. Development of a more optimum precipitate distribution was crudely attempted in a 0.018-in.-thick specimen by increasing the nitrogen pressure in steps from 50 to 760 Torr during a 24-hr anneal at 1260°C. The HfN particle size was more uniform, and the particles at the center, 0.009 in. below the surface shown in Fig. 36, were smaller than those at a corresponding depth in the 0.050-in.-thick specimen nitrided at the same temperature. In addition, no evidence of subsurface particle coarsening was observed in this specimen. As shown in Figs. 34 and 35, the tensile strength of this specimen at 1370°C was superior to that of the other nitrided specimens. The improvements in structure and tensile strength obtained in this specimen may have been determined more by the decreased thickness and reduced time at the nitriding temperature than by the variation in nitrogen pressure.

Fig. 36. Transmission electron micrograph of precipitates and substructure at the center of 0.018-in-thick specimen other nitriding at 1260°C.

Conclusions

1. Internal nitriding of a Mo-1 at.% Hf alloy produces high-temperature tensile strengths substantially superior to those currently available in commercial, Mo-base refractory alloys.

2. The major contribution to the strengthening by internal nitriding arises from a homogeneous dispersion of coherent platelike HfN precipitates oriented on {001} planes of the Mo matrix.

3. An additional strengthening contribution can be obtained from a work-hardened dislocation substructure developed by prior mechanical working and stabilized at high temperatures by the HfN dispersion.

4. Growth of the HfN particles during internal nitriding occurs principally by Ostwald ripening at the nitriding front which produces an increase in average particle size with increasing depth below the external surface.

5. The HfN particles grow in a coherent manner. Thickening of the

plate-like particles occurs by the nucleation and growth of coherent ledges on the planar surfaces. This thickening process produces an increase in the peripheral coherency strain which is relaxed by the formation of intrinsic dislocation loops within the particle by the coalescence of vacancies.

6. A severe particle-coarsening mechanism occurs at high temperatures in regions of the nitrided alloys containing a high density of small, fully coherent HfN particles. The coarsening occurs by the migration of grain boundaries which sweep up the small fully coherent particles, the components of which then feed large semi-coherent particles growing behind the boundary. The driving force for this process is the recovery of the matrix strain energy around the small fully coherent precipitate.

Acknowledgments

The authors wish to express their appreciation to Sam DiGiallonardo and C. J. Echer for the metallography and electron micrographs contained in this report.

References

1. A. K. Mukherjee and J. W. Martin, "Hardening of Molybdenum-Titanium Alloy by Nitride Dispersions," J. Less Common Metals, 2, 362 (1960); and A. K. Mukherjee and J. W. Martin, "Hardening of Molybdenum-Zirconium Alloy by Nitride Dispersions," J. Less Common Metals, 3, 216 (1961).
2. N. E. Ryan and J. W. Martin, "Hardening of Some Molybdenum-Based Alloys by Precipitation of Nitride and Carbide Phases," Proc. 6th Plansee Society Seminar for Powder Metallurgy, Ruette, Tyrol, Austria, CFSTI No. N69-00661 (June 1960).
3. R. A. Rapp, "Kinetics, Microstructures and Mechanism of Internal Oxidation in High-Temperature Alloy Oxidation," Corrosion, 21, 382 (Dec. 1965).
4. P. B. Hirsch, A. Howie, R. B. Nicholson and D. W. Pashley, Electron Microscopy of Thin Crystals (Butterworth, Washington, D.C., 1965), p. 332.
5. D. Mosher, C. Collins and C. Wert, "Clustering of Zr and N in Nb," Acta Met. 18, 797 (1970).

Printed in USA. Available from the National Technical Information Center, National Bureau of Standards, U. S. Department of Commerce, Springfield, Virginia 22151
Price: Printed Copy $3.00; Microfiche $0.65.